Since January 2020 Elsevier has created a COVID-19 resource centre with free information in English and Mandarin on the novel coronavirus COVID-19. The COVID-19 resource centre is hosted on Elsevier Connect, the company's public news and information website.

Antiviral Research 190 (2021) 105064

Contents lists available at ScienceDirect

Antiviral Research

journal homepage: www.elsevier.com/locate/antiviral

Proteomic analysis identifies the RNA helicase DDX3X as a host target against SARS-CoV-2 infection

Fabiola Ciccosanti [a,1], Martina Di Rienzo [a,1], Alessandra Romagnoli [a,1], Francesca Colavita [a], Giulia Refolo [a], Concetta Castilletti [a], Chiara Agrati [a], Annalaura Brai [b], Fabrizio Manetti [b], Lorenzo Botta [c], Maria Rosaria Capobianchi [a], Giuseppe Ippolito [a], Mauro Piacentini [a,d,*], Gian Maria Fimia [a,e,**]

[a] Department of Epidemiology, Preclinical Research and Advanced Diagnostics, National Institute for Infectious Diseases 'L. Spallanzani' IRCCS, Rome, Italy
[b] Department of Biotechnology, Chemistry and Pharmacy, University of Siena, Siena, Italy
[c] Department of Ecological and Biological Sciences, University of Tuscia, Viterbo, Italy
[d] Department of Biology, University of Rome 'Tor Vergata', Rome, Italy
[e] Department of Molecular Medicine, Sapienza University of Rome, Rome, Italy

ARTICLE INFO

Keywords:
Antiviral drugs
COVID-19
Proteomics
Stress granules
DEAD RNA helicase
G3BP1

ABSTRACT

COVID-19 is currently a highly pressing health threat and therapeutic strategies to mitigate the infection impact are urgently needed. Characterization of the SARS-CoV-2 interactome in infected cells may represent a powerful tool to identify cellular proteins hijacked by viruses for their life cycle and develop host-oriented antiviral therapeutics.

Here we report the proteomic characterization of host proteins interacting with SARS-CoV-2 Nucleoprotein in infected Vero E6 cells. We identified 24 high-confidence proteins mainly playing a role in RNA metabolism and translation, including RNA helicases and scaffold proteins involved in the formation of stress granules, cytoplasmic aggregates of messenger ribonucleoproteins that accumulate as a result of stress-induced translation arrest. Analysis of stress granules upon SARS-CoV-2 infection showed that these structures are not induced in infected cells, neither eIF2α phosphorylation, an upstream event leading to stress-induced translation inhibition. Notably, we found that G3BP1, a stress granule component that associates with the Nucleoprotein, is required for efficient SARS-CoV-2 replication. Moreover, we showed that the Nucleoprotein-interacting RNA helicase DDX3X colocalizes with viral RNA foci and its inhibition by small molecules or small interfering RNAs significantly reduces viral replication.

Altogether, these results indicate that SARS-CoV-2 subverts the stress granule machinery and exploits G3BP1 and DDX3X for its replication cycle, offering groundwork for future development of host-directed therapies.

Abbreviations: CoV, coronavirus; COVID-19, coronavirus disease 2019; DDX, DEAD-box helicase; DHX, DEAH box protein; DMVs, double-membrane vesicles; eIF, Eukaryotic initiation factor; ERGIC, ER-Golgi intermediate compartment; G3BP, Ras-GAP SH3 domain binding protein; GAPDH, Glyceraldehyde 3-phosphate dehydrogenase; GSK3, Glycogen synthase kinase 3; HBV, hepatitis B virus; HCV, hepatitis C virus; HIV-1, human immunodeficiency virus type 1; hnRNPA1, heterogeneous nuclear ribonucleoprotein A1; IGF2BP, Insulin-like growth factor 2 mRNA-binding protein; LDH, Lactate dehydrogenase; MEM, Modified Eagle Medium; NSPs, non-structural proteins; PABPC3, Polyadenylate-binding protein 3; PP1, Protein phosphatase 1; qRT-PCR, quantitative reverse transcription polymerase chain reaction; SARS-CoV-2, severe acute respiratory syndrome-related coronavirus 2; SDS PAGE, Sodium Dodecyl Sulphate; PolyAcrylamide Gel Electrophoresis, siRNA; small interfering RNA, SPFQ; Splicing factor, proline- and glutamine-rich protein; SYNCRIP, Synaptotagmin Binding Cytoplasmic RNA Interacting Protein; TMPRSS2, transmembrane serine protease 2; YBX1, Y-box-binding protein 1.

* Corresponding author. Department of Biology, University of Rome 'Tor Vergata', Via della Ricerca Scientifica 1, 00133 Rome, Italy.
** Corresponding author. Department of Molecular Medicine, Sapienza University of Rome, Viale Regina Elena 324, 00161 Rome, Italy.
E-mail addresses: mauro.piacentini@uniroma2.it (M. Piacentini), gianmaria.fimia@inmi.it (G.M. Fimia).
[1] these authors contributed equally to this work.

https://doi.org/10.1016/j.antiviral.2021.105064
Received 1 October 2020; Received in revised form 9 March 2021; Accepted 13 March 2021
Available online 26 March 2021

1. Introduction

As every obligate intracellular parasite, SARS-CoV-2, the causative agent of COVID-19, needs to hijack a large series of host factors to facilitate its replication (de Wilde et al., 2018; Fung and Liu, 2019). Moreover, SARS-CoV-2 has to establish interactions with a complex network of host antiviral pathways in order to inhibit or subvert them (Sa Ribero et al., 2020; Lei et al., 2020). In-depth understanding of SARS-CoV-2-host interaction is therefore critical to identify cellular factors that play a role in SARS-CoV-2 infection, and develop novel antiviral strategies to limit virus spreading.

Current information on SARS-COV-2 interactions with host cells is mainly inferred from studies on related coronaviruses, with a rapidly increasing number of new studies that are confirming these findings in SARS-COV-2 or underlining differences (Hartenian et al., 2020).

SARS-COV-2 enters the cells through the binding of the Spike protein to the receptor ACE2 by either direct membrane fusion or endocytosis (Hoffmann et al., 2020). In the former case, after binding ACE2, the membrane fusion activity of the Spike protein is triggered by a proteolytic cleavage mediated by the transmembrane serine protease 2 (TMPRSS2). In the latter case, once endocytosed, Spike is activated by cathepsins in a pH-dependent manner, which can be inhibited by lysosomotropic agents (Pislar et al., 2020; Sauvat et al., 2020). After uncoating, the polyprotein 1a/1b is translated from the genomic RNA and processed into 11 non-structural proteins (NSPs), including the RNA-dependent RNA polymerase (NSP12) and a small number of co-factors for viral replication. These proteins mediate the synthesis of the negative strand RNA that, in turn, serves as a template for generation of positive strand progeny genomes (Fung and Liu, 2019; Hartenian et al., 2020; Ortiz-Prado et al., 2020). The replication complex localizes to modified host membranes including double-membrane vesicles (DMVs) that are derived from the endoplasmic reticulum (Snijder et al., 2020).

Viral and host RNA-binding proteins have been identified in association with the viral genome and contribute to driving translation and replication. For instance, phosphorylation of the SARS-CoV Nucleoprotein mediated by the host protein kinase GSK3 recruits the DEAD-box helicase 1 (DDX1) to the viral genome to facilitate template read-through during viral replication (Wu et al., 2014). The RNA-binding protein hnRNPA1 also tightly binds to SARS-CoV Nucleoprotein and regulates viral RNA synthesis (Luo et al., 2005).

Subgenomic RNAs are also obtained during replication by discontinuous transcription (Kim et al., 2020), which encode for the structural proteins Spike, Membrane, Envelope, and Nucleoprotein, required for viral particle assembly and release (Siu et al., 2008), as well as accessory proteins (ORFs 3–9), not required for viral replication but responsible for the modulation of host antiviral response (Liu et al., 2014). Particle assembly occurs in the ER-Golgi intermediate compartment (ERGIC) and trafficked via the secretory pathway to be released by exocytosis (Stertz et al., 2007).

Interestingly, sequence alignment of different Coronaviruses shows that the structural proteins are less conserved than the non-structural proteins, suggesting that the former are more diverse in need of adaptation to new hosts, which prioritize their study to understand the unique feature of SARS-CoV-2 (Cui et al., 2019).

A proteomic characterization on SARS-CoV-2 interactome upon ectopic expression of individual viral proteins has been recently reported (Gordon et al., 2020), providing crucial information on host processes that are targeted by SARS-CoV-2, most of which remain to be validated in infected cells to elucidate their functional role. To deepen the knowledge of the molecular mechanisms underlying SARS-CoV-2 infection, we have carried out a mass spectrometry analysis of host proteins interacting with SARS-CoV-2 Nucleoprotein in infected Vero E6 cells.

2. Materials and methods

2.1. Cell culture and treatments

Vero E6 cells (ATCC CRL-1586) were maintained in Modified Eagle Medium (MEM, Sigma Aldrich, M2279) supplemented with 10% heat inactivated fetal bovine serum (Gibco, 10270), 2 mM L-glutamine, and 1% penicillin/streptomycin solution (Sigma-Aldrich, G7513; P0781) at 37 °C in a humidified atmosphere of 5% CO_2. Calu-3 (ATCC HTB-55) were maintained in RPMI-1640 MEDIUM (Sigma Aldrich, R0883) supplemented as for MEM. Cells were screened for mycoplasma contamination by PCR (ABMgood, G238). Cells were exposed to SARS-CoV-2 isolate (2019-nCoV/Italy-INMI1, available from EVAg, Ref-SKU: 008V-03893, and from GISAID accession number EPI_ISL_410546) in medium without FBS for 1 h at 37 °C at a multiplicity of infection (MOI) 0.01 or 0.001. At the end of the adsorption period, cells were washed and incubated in medium with 2%FBS, and where indicated, treated with RK-33 (S8246, Selleckchem) or C-4b (Maga et al., 2011) at the indicated concentrations.

For siRNA experiments, Vero E6 cells were transiently transfected with specific RNA oligonucleotides and Lipofectamine RNAimax (Life Technologies, 13778150), as indicated by the supplier. The sequences of siRNA used were as follows: G3BP1a (Life Technologies, HSS115445 CCAAGAUGAGGUCUUUGGUGGGUUU), G3BP1b (Life Technologies, HSS115446 ACAUUUAGAGGAGCCUGUUGCUGAA), DDX3Xa (Life Technologies, HSS102714 CCUAGACCUGAACUCUUCAGAUAAU), DDX3Xb (Life Technologies, HSS176054 CACCAACGAGAGAGUUGGCAGUACA). Stealth RNAi™ siRNA Negative Control, Med GC (Life Technologies, 1293530) were used as negative control.

2.2. qRT-PCR and viral titration

Viral RNA was extracted from Vero E6 and Calu-3 cells using Trizol (Life Technologies, 15596018), according to the manufacturer's instructions. Extracellular RNA was purified as described (Refolo et al., 2019).

SARS-CoV-2 RNA was amplified by quantitative RT-PCR (qRT-PCR) in Rotor-GeneQ Real-Time cycler (Qiagen) using RealStar® SARS-CoV-2 RT-PCR Kit 1.0 (Altona Diagnostic GmbH) or by using a reverse transcription kit (Promega, A3500) cDNA synthesis and Maxima SYBR Green/ROX qPCR Master Mix (Thermo Scientific, K0253), as previously described (Refolo et al., 2019). In latter case, primer sets for all amplicons were designed using the PrimerQuest software (IDT): SARS-CoV-2 env forward CTTCGATTGTGTGCGTACT and reverse ACCAGAAGATCAGGAACTCTA; L34 forward GTCCCGAACCCCTGGTAATAG; L34 reverse GGCCCTGCTGACATGTTTCTT; DDX3X forward CTTGGCTGTAGGAAGAGTTG; DDX3X reverse TCCTTGCCTGTTGCATTTA; G3BP1 forward AGCCTGAGCCAGTATTAGA; G3BP1 reverse GTCACAGATGCCCAAGAAA. Levels of viral RNAs were normalized to the housekeeping gene L34 level using equation $2^{-\Delta Ct}$.

Viral titers upon drug treatments were determined by limiting dilution assay and residual infectivity was expressed as 50% Tissue Culture Infective Dose (TCID50/ml) calculated according to the Reed and Muench method. For this analysis, cells and culture media were collected at 24h post infection and subjected to repeated freezing and thawing cycles. Clarified supernatants were applied at serial 5-fold dilutions on Vero E6 cells and serial 3-fold dilutions on Calu-3 cells seeded in 96-well plates at 30,000 cells/well and cytopathic effects were evaluated after 5 days.

2.3. Immunoprecipitation and protein analysis

Immunoprecipitation and immunoblotting were performed as previously described (Di Rienzo et al., 2019). Briefly, cells were lysed lysing

in Tris buffer: 10 mM Tris pH 8.0 (Santa Cruz Biotechnology, sc-3715A), 150 mM NaCl (Sigma-Aldrich, S7653), 10% glycerol (Sigma-Aldrich, G7757), 1% Triton-X100 (Sigma-Aldrich, T9284) complemented with protease and phosphatase inhibitors [Protease Inhibitor Cocktail plus (Sigma-Aldrich, P8340), 5 mM sodium fluoride (Sigma-Aldrich, S-7920), 0.5 mM sodium orthovanadate (Sigma-Aldrich, S6508), 1 mM sodium molybdate (Sigma-Aldrich, S-6646) and 0.5 mM phenylmethylsulfonyl fluoride (Sigma-Aldrich, P7626)]. For viral and cellular protein immunoprecipitation, protein extracts were incubated overnight with 5 μg of antibody, and immunocomplexes were recovered using 40 μl of Protein A Sepharose (GE Healthcare, GE 17-1279-01) or Protein G Sepharose (GE Healthcare, GE 17-0618-01). Immunocomplexes and protein total extracts were separated on SDS PAGE gels and electroblotted onto nitrocellulose (Whatman Amersham, 10600041) or PVDF (Millipore, IPVH20200) membranes. Blots were incubated with primary antibodies in 5% nonfat dry milk (Biosigma, 711160) or Bovine Serum Albumin (BSA) (Sigma-Aldrich, A9647) in PBS (Thermo Fisher Scientific, 18912-0149) plus 0.1% Tween-20 (Sigma-Aldrich, P1379) overnight at 4 °C. The primary antibodies used in this study were: SARS-CoV Nucleocapsid Rabbit (200-401-A50, Rockland Immunochemicals), SARS-CoV Nucleocapsid Mouse [6H3] (GTX632269, GENETEX), SARS-CoV-2 NSP8 [5A10] (GTX632696 GENETEX), SARS-CoV-2 ORF7a [3C9] (GTX632602, GENETEX), PARP antibody (BK9542S, Cell Signaling), anti-HSP90 alpha/beta (F-8) (sc-13119, Santa Cruz Biotech), anti-GAPDH (glyceraldehyde-3-phosphate dehydrogenase) (Millipore, CB1001), DDX3X Rabbit (A5637, ABCLONAL), DDX3 Mouse (A10099, ABCLONAL), G3BP1 Rabbit (13057-2-AP, Proteintech), SARS-CoV SPIKE [1A9] (GTX632604, GENETEX), dsRNA Mouse (10010200, SCICONS J2). Detection was achieved using horseradish peroxidase–conjugated secondary antibodies [anti-rabbit 711-036-152 and anti-mouse 715-036-150 (Jackson ImmunoResearch Laboratories)] and enhanced chemiluminesence (ECL) [Immobilon Classico WBLUC0500 and Immobilon Crescendo Western HRP substrate WBLUR0500 (Millipore)]. Signals were acquired using a ChemiDoc imaging system (Bio-Rad).

2.4. Confocal microscopy

Cells were fixed with 4% paraformaldehyde (CARLO ERBA Reagents, 387507) in PBS followed by permeabilization with 0.2% Triton X-100 (Sigma-Aldrich, T9284) in PBS. Cells were then labeled with the primary antibody anti-SARS-CoV Nucleocapsid Mouse [6H3] (GTX632269, GENETEX), SARS-CoV SPIKE [1A9] (GTX632604, GENETEX), dsRNA Mouse (10010200, SCICONS J2), DDX3X Rabbit (A5637, ABCLONAL), DDX3 Mouse (A10099, ABCLONAL), G3BP1 Rabbit (13057-2-AP, Proteintech) for 1 h at room temperature and visualized by means of Cy3 (jg715-156-150, Jackson ImmunoResearch) or Alexa Fluor 488 (A21206, Life Technologies) conjugated secondary antibodies. Coverslips were mounted in Prolong Gold antifade (P36935, Life Technologies) and examined under a confocal microscope (Leica TCS SP2). Digital images were acquired with the Leica software and the image adjustments and merging were performed by using the appropriated tools of ImageJ software. Quantification of colocalization, expressed in terms of Mander's overlap coefficient, was calculated using the JacoP plugin of ImageJ software, as previously described(Romagnoli et al., 2018). A minimum of 50 cells per sample experimental condition were counted for triplicate samples per condition in each experiment.

2.5. Immunoprecipitation and LC-MS/MS analysis

Immunocomplexes, purified as described above, were eluted twice with 0.5 M NH_4OH (Sigma-Aldrich, 338818), 0.5 mM EDTA (443885J, BDH). The first and second elutions of each immunoprecipitation were pooled, dried, resuspended in NH_4HCO_3, boiled at 95 °C. Disulfide bonds were reduced and alkylated, respectively with 10 mM dithiothreitol at 56 °C, and 55 mM iodoacetamide at RT. After precipitation with ethanol 100%, the samples were resuspended in NH_4HCO_3 50 mM, 2M urea and were digested by trypsin (0.2μg/sample) at 37 °C overnight. Then peptides were purified through the filter of a Zip-Tip (C-18 Resin, ZTC18S096, Millipore), eluted with 80% acetonitrile and 0.1% TFA, dried and resuspended in 2.5% acetonitrile, 0.1% TFA, 0.1% formic acid. The peptide mixture were analyzed by ultra-high performance liquid chromatography coupled with high resolution mass spectrometry using Thermo Scientific Q Exactive Plus Orbitrap; in particular, the peptides were separated by nano liquid chromatography (UltiMate 3000 RSLC nano-LC system, Thermo Fisher Scientific), loaded onto a 75 μm C18 column (ES800 - Thermo Fisher Scientific), using a 100 min multistep gradient elution (from 4 to 90% eluent B with a constant flow of 0.3 μL/min), and were analyzed by Exactive Q plus mass spectrometer (Thermo Fisher Scientific). The raw data from the mass spectrometric analysis were processed using the MaxQuant software v.1.5.5.1. Proteomic experiments were performed twice in duplicate. Data were analyzed with the Perseus software v.1.6.12 to select proteins that were reproducibly identified to be associated with the SARS-CoV-2 nucleoprotein, as previously described(Tyanova et al., 2016). Analysis of biological processes associated to the identified interacting proteins was carried out with the STRING software (Szklarczyk et al., 2019).

2.6. Statistical analysis

Statistical analysis of immunoblotting and PCR was performed using unpaired, two-tailed Student's t-test (Excel software). Values are shown as mean±standard deviation of three independent experiments. Confocal data analysis was performed using a non-parametric two-tailed Mann-Whitney *U* test (GraphPad Prism). Values are shown as mean±standard error of the mean of three independent experiments. P-values <0.05 were marked by *, $p < 0.01$ = **, $p < 0.001$ = ***. Densitometric analysis of immunoblots was performed using the Adobe Photoshop software. The control ratio was arbitrarily defined as 1.00. No exclusion criteria were applied to exclude samples from analysis. Samples were not randomized. Normal distribution for *t*-test analysis was assumed based on the appearance of the data, since $n < 5$. Statistical methods were not used to predetermine sample sizes and investigators were not blinded to group allocation or when assessing the outcome.

3. Results

3.1. Analysis of nucleoprotein interactome in SARS-CoV-2 infected Vero E6 cells

Vero E6 cells were infected with SARS-CoV-2 at multiplicity of infection (MOI) 0.01, lysed after 24 h and protein extracts were subjected to immunoprecipitation using an anti-Nucleoprotein antibody (Fig. 1A). Purified proteins were tryptic digested and analyzed by mass spectrometry. Results from two experiments performed in duplicate identified a list of 24 cellular proteins and 3 viral proteins that specifically interact with the Nucleoprotein (Fig. 1B and Tables S1 and S2). Similar to what reported for other Coronaviruses, Nucleoprotein was found in association with the structural proteins Membrane and Spike, and the non-structural proteins NSP3 and NSP4 (Table S1), which are transmembrane proteins involved in both viral polyprotein cleavage and membrane rearrangement to form DMVs (Hartenian et al., 2020). Among the interacting host factors, we identified: 11 ribosomal proteins, the ribosome biogenesis factor LSG1 and a series of RNA-binding factors involved in cytoplasmic regulatory processes of mRNA metabolism (Fig. 1C), including the mRNA transport proteins HNRNPA1, SYNCRIP, SPFQ and PABPC3, the scaffold factors involved in cytoplasmic RNA storage G3BP1, G3BP2, IGF2BP2, IGF2BP3, YBX1, the ATP-dependent RNA helicases DDX3X and DHX9, and the beta catalytic subunit of the serine/threonine-protein phosphatase 1 (PP1) (Tables S2 and S3). A common trait shared by the identified factors interacting with Nucleoprotein is their involvement in stress granules, aggregate structures

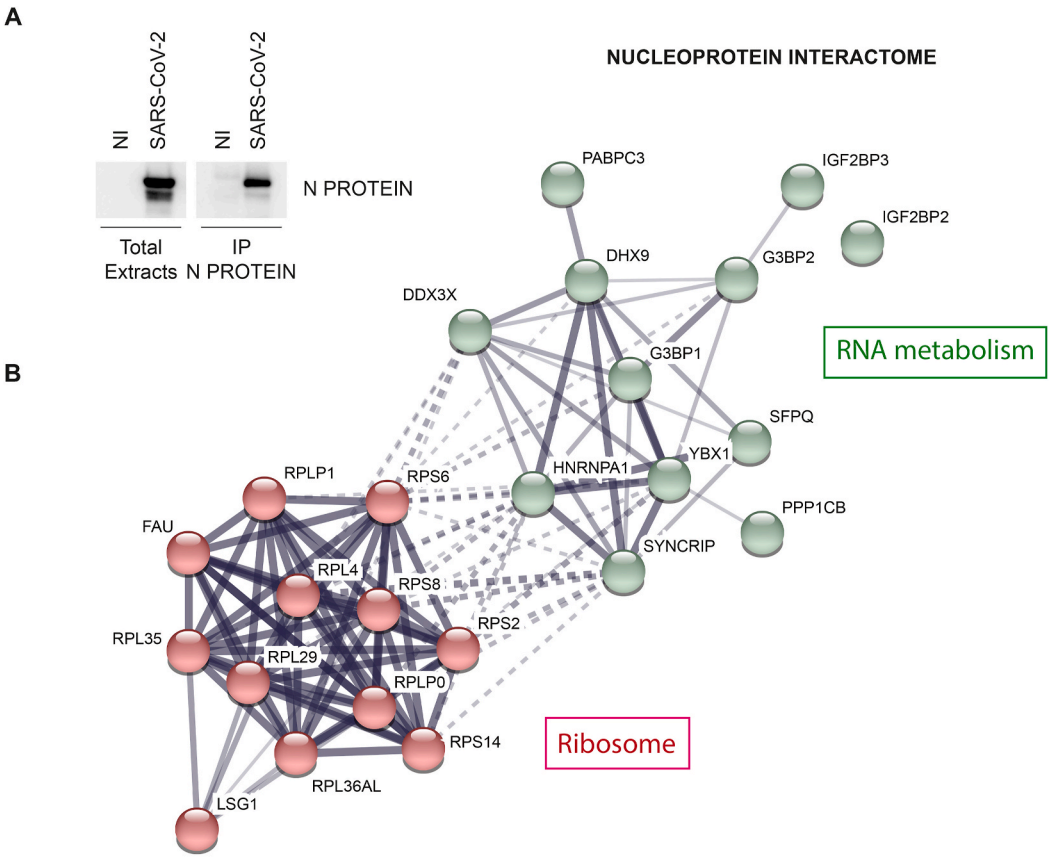

C

Biological Process (GO)			
GO term	*description*	*count in gene set*	*false discovery rate*
GO:0016071	mRNA metabolic process	16 of 667	1.77e-15
GO:0006413	translational initiation	11 of 142	4.07e-15
GO:0006614	SRP-dependent cotranslational protein targeting to membrane	10 of 92	4.45e-15
GO:0006412	translation	13 of 362	8.63e-15
GO:0000184	nuclear-transcribed mRNA catabolic process, nonsense-mediated decay	10 of 118	1.69e-15

Fig. 1. Characterization of SARS-CoV-2 Nucleoprotein interactome. A) Vero E6 cells were infected with the SARS-CoV-2 isolate (2019-nCoV/Italy-INMI1) for 1 h at 37 °C at a multiplicity of infection (MOI) 0.01. At 24 h post infection, cells were harvested and protein extracts were subjected to immunoprecipitation using an anti-SARS-CoV Nucleoprotein antibody. Immunopurified complexes were analyzed by immunoblotting. NI: non-infected; N PROTEIN: Nucleoprotein. **B)** Network of Nucleoprotein interacting proteins generated with STRING, with continuous lines to represent direct interactions (physical), while dotted lines to represent indirect ones (functional). Line thickness indicates the strength of data support between edges. **C)** Top five biological processes enriched in Nucleoprotein interacting proteins based on gene ontology terms, generated with STRING.

composed of proteins and RNA molecules that usually are formed to stall translation initiation in a reversible manner upon cellular stress (McCormick and Khaperskyy, 2017; Protter and Parker, 2016). This finding prompted us to verify how SARS-CoV-2 infection impacts on the presence of stress granules.

3.2. The stress granule component G3BP1 is a Nucleoprotein interacting protein required for SARS-CoV-2 replication

First, we verified the interaction of Nucleoprotein with the stress granule component G3BP1 in SARS-CoV-2 infected cells by

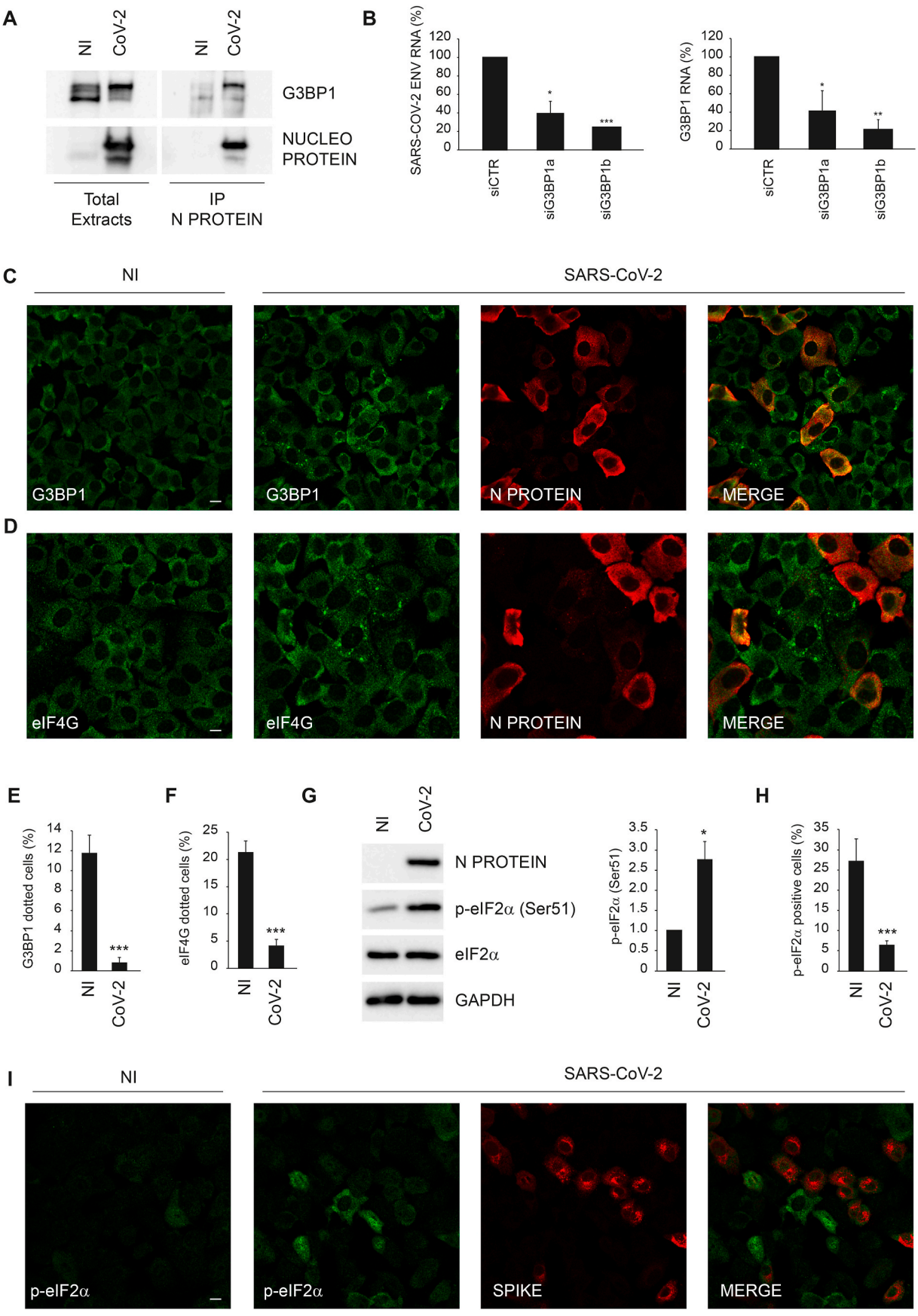

(caption on next page)

Fig. 2. SARS-CoV-2 Nucleoprotein interacts with G3BP1. A) Vero E6 cells infected with SARS-CoV-2 at MOI 0.01 were harvested after 24 h and protein extracts were subjected to immunoprecipitation using an anti-SARS-CoV Nucleoprotein antibody. Immunopurified complexes were analyzed by immunoblotting using anti-SARS-CoV Nucleoprotein and anti-G3BP1 antibodies. **B)** Vero E6 cells were transfected with small interfering RNAs specific for G3BP1 (siG3BP1a and siG3BP1b) and infected with SARS-CoV-2 at MOI 0.001. Twenty-four hours later, cells were harvested and G3BP1 and viral RNAs were analyzed by RT-qPCR. The graphs report means ± SD of normalized values from three independent experiments. * = $p < 0.05$, ** = $p < 0.01$, *** = $p < 0.001$. Viral RNA levels are reported as fold changes with respect to the amount detected at 24h post infection **C–F)** Vero E6 cells infected with SARS-CoV-2 at MOI of 0.01 were fixed after 24 h and analyzed for G3BP1 (C,E) or eIF4G (D,F) localization by immunofluorescence using specific antibodies. Anti-SARS-CoV Nucleoprotein antibody were also used to detect SARS-CoV-2 positive cells. The graphs in (E) and (F) report means ± SEM of percentage of G3BP1 or eIF4G dotted cells among uninfected and infected cells from three independent experiments. *** = $p < 0.001$. **G)** Vero E6 cells infected with SARS-CoV-2 MOI 0.01 were harvested after 24 h and SARS-CoV-2 Nucleoprotein, eIF2α and p-eIF2α levels were analyzed by immunoblotting. GAPDH was included as a loading control. The graph reports means ± SD of p-eIF2α/eIF2α values from three independent experiments. * = $p < 0.05$. Protein levels are reported as fold changes with respect to the non-infected cells. **H–I)** Vero E6 cells infected with SARS-CoV-2 at MOI 0.01 were fixed after 24 h and analyzed for p-eIF2α localization by immunofluorescence using a specific antibody (i). Anti-SARS-CoV SPIKE antibody was also used to detect SARS-CoV-2 positive cells. The graph in (H) reports means ± SEM of percentage of p-eIF2α positive cells among uninfected and infected cells from three independent experiments. *** = $p < 0.001$. NI: non-infected; N PROTEIN: Nucleoprotein; CoV-2: SARS-CoV-2. Scale bar, 10 μm.

immunoprecipitation using an anti-Nucleoprotein antibody different from that used in the mass spectrometry analysis. Immunoblotting analysis of Nucleoprotein associated proteins confirmed its interaction with G3BP1 (Fig. 2A). Then, we asked whether G3BP1 is a host factor required for SARS-CoV-2 replication using a RNA interference approach. Vero E6 cells were transfected with short interfering RNA duplexes (siRNA) specific for G3BP1, or non-targeting siRNA as negative control, and infected with SARS-CoV-2 at MOI 0.001. Twenty-four hours later, cells were harvested and intracellular viral RNA analyzed by RT-qPCR. As shown in Fig. 2B, SARS-COV-2 RNA levels are significantly reduced when G3BP1 expression was downregulated, suggesting that Nucleoprotein targets G3BP1 to favour viral replication.

Since that Nucleoprotein was found to interact with several components of stress granules, we asked if SARS-CoV-2 infection impacts on the formation of these cytoplasmic bodies. To this aim, the presence of stress granules was evaluated by monitoring the subcellular distribution of G3BP1 by confocal microscopy. We observed that most of the infected cells have a diffuse staining of G3BP1 (Fig. 2C,E). Conversely, we found that a dotted staining of G3BP1 is present in approx. 10% of non-infected cells of the same cell population. This result was also confirmed when stress granules are visualized by using an antibody against eIF4G, an eukaryotic initiation factor that is sequestered within stress granules (McCormick and Khaperskyy, 2017; Protter and Parker, 2016) but that was not detected in the Nucleoprotein interactome (Fig. 2D,F). In addition, we assessed if the SARS-CoV-2 infection triggers the phosphorylation of the eukaryotic initiation factor 2 alpha (p-eIF2α), an upstream event in the induction of stress granule formation (McCormick and Khaperskyy, 2017; Protter and Parker, 2016). Immunoblotting analysis showed that p-eIF2α level is increased upon SARS-CoV-2 infection (Fig. 2G); however, confocal microscopy indicated that this increase is mainly restricted to non-infected cells (Fig. 2H and I). Altogether, these results indicate that SARS-CoV-2 infection prevents p-eIF2α and the formation of stress granules possibly to avoid protein translation arrest, while neighbouring non-infected cells receive alarm signals that promote this event.

3.3. The RNA helicase DDX3X is a host target of nucleoprotein required for SARS-CoV-2 replication

Next, we investigated if Nucleoprotein interacts with "druggable" host factors critical for SARS-CoV-2 replication. We decided to focus on the role of the RNA helicase DDX3X for two main reasons: a) a proviral role of DDX3X, associated to its ability to unfold viral RNA secondary structures (Kukhanova et al., 2020), has been reported for numerous viruses, including West Nile and HIV-1 (Brai et al., 2019, 2020); b) specific inhibitors of DDX3X with antiviral activity are currently available (Maga et al., 2011; Brai et al., 2020).

First, we verified the interaction of Nucleoprotein with DDX3X in SARS-CoV-2 infected cells by immunoprecipitation using an anti-Nucleoprotein antibody different from that used in the mass spectrometry analysis. Immunoblotting analysis of Nucleoprotein associated proteins confirmed the binding with DDX3X (Fig. 3A). DDX3X-Nucleoprotein interaction was also confirmed in reverse co-immunoprecipitation by using an anti-DDX3X antibody (Fig. 3B). Then, we assessed if DDX3X is recruited to the replication complex by analysing the colocalization with the SARS-CoV-2 genome by confocal microscopy using an anti-double strand RNA (dsRNA) antibody commonly used to detected positive strand RNA viruses (Weber et al., 2006). As shown in Fig. 3C and Figure S1A, DDX3X staining partially overlaps with the viral RNA, suggesting that DDX3X is recruited to the viral replication sites. The specificity of dsRNA antibody in detecting the viral genome was verified by staining uninfected cells (Figure S1B).

Then, we asked whether DDX3X is a host factor required for SARS-CoV-2 replication using a RNA interference approach. Vero E6 cells were transfected with short interfering RNA duplexes (siRNA) specific for DDX3X, or non-targeting siRNA as negative control, and infected with SARS-CoV-2 at MOI 0.001. Twenty-four hours later, cells were harvested and intracellular viral RNA analyzed by RT-qPCR. As shown in Fig. 3D, SARS-COV-2 RNA levels are significantly reduced when DDX3X expression was downregulated, suggesting that Nucleoprotein recruits DDX3X to the replication complex for novel virus production.

3.4. DDX3X inhibitors impair SARS-CoV-2 replication in Vero E6 and Calu-3 cells

Prompted by these results, we assessed if DDX3X is required for SARS-CoV-2 infection by using two specific inhibitors of DDX3X, the diazepine derivative RK-33 (Yang et al., 2020) and the rhodanine Compound 4B (C–4B) (Maga et al., 2011) (Fig. 4A). Vero E6 cells were infected with SARS-CoV-2 at MOI 0.001 for 1 h followed by incubation with the RK-33 or C–4B compounds for 24 h. The amount of intracellular virus was monitored by RT-qPCR and immunoblotting. As shown in Fig. 4B,D, the levels of viral RNA and two viral proteins, NSP8 and ORF7a, are significantly reduced in cells treated with DDX3X inhibitors. No cytopathic effects were observed when cells were treated with these compounds, as shown by monitoring both necrosis (LDH release, data not shown) and apoptosis (cleaved PARP, Fig. 4C, compare lane 1, 5 and 6). In addition, a complete inhibition of SARS-CoV-2-induced apoptosis was observed when cells were treated with RK-33 or C–4B, as shown by cleaved PARP immunoblotting (Fig. 4C, compare lane 2, 3 and 4). The effect of DDX3X inhibitors on SARS-CoV-2 replication was confirmed when the infectivity of viral particles produced in cells treated with different concentrations of RK-33 or C–4B was measured by limiting dilution assay (Fig. 4E).

Finally, we evaluated the ability of DDX3X inhibitors to affect SARS-CoV-2 replication in human cells. To this aim, the lung adenocarcinoma cell line Calu-3 was infected with SARS-CoV-2 at MOI 0.001 for 1 h followed by incubation with the RK-33 or C–4B compounds at 3 different concentrations for 24 h. No cytopathic effects were observed at any drug concentration (data not shown). The analysis of intracellular and extracellular viral RNA by RT-qPCR confirmed that both DDX3X inhibitors impairs SARS-CoV-2 replication in a dose dependent manner (Fig. 5A and

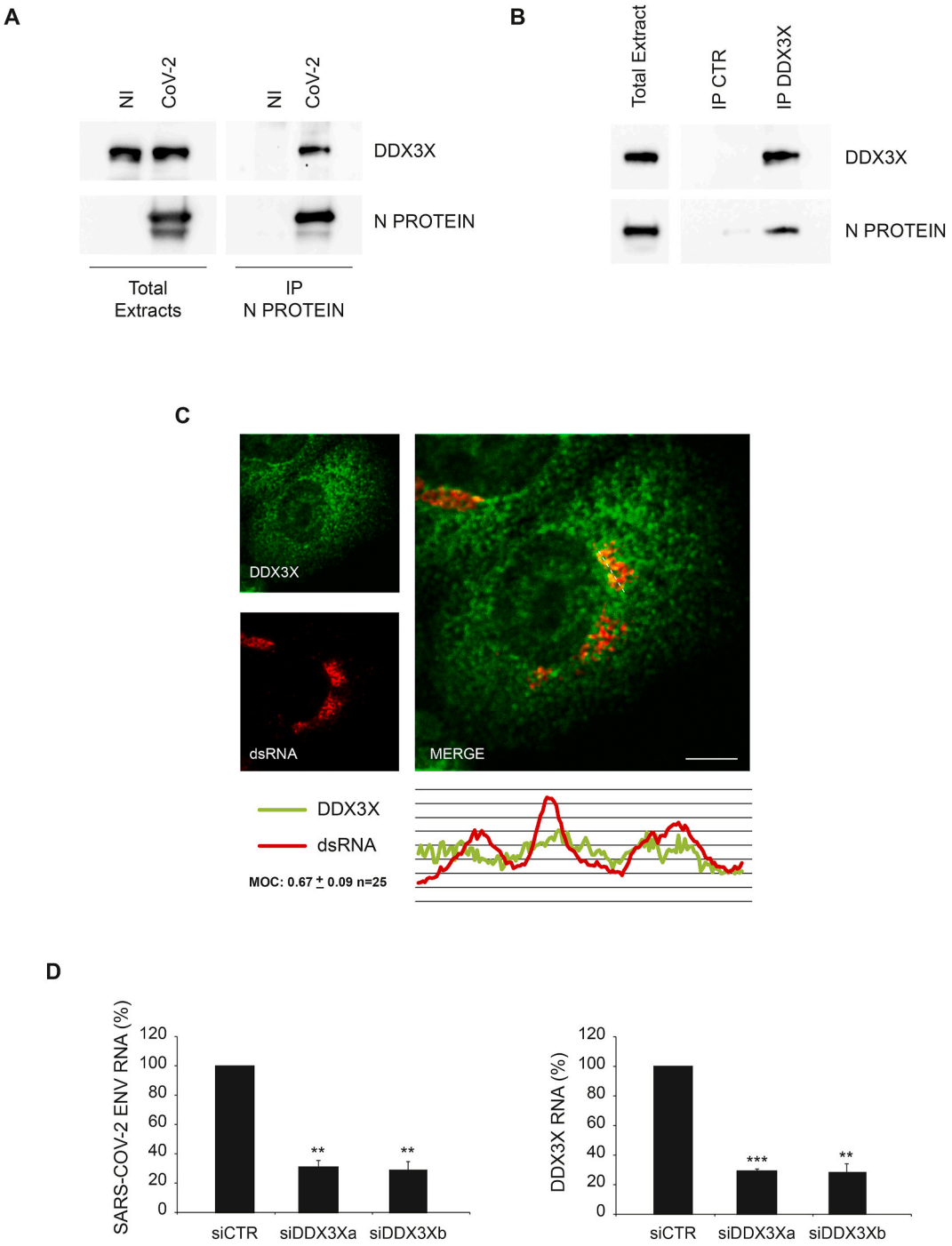

Fig. 3. SARS-CoV-2 Nucleoprotein interacts with DDX3X. A) Vero E6 cells infected with SARS-CoV-2 at MOI 0.01 were harvested after 24 h and protein extracts were subjected to immunoprecipitation using an anti-SARS-CoV Nucleoprotein antibody. Immunopurified complexes were analyzed by immunoblotting using anti-SARS-CoV Nucleoprotein and anti-DDX3X antibodies. **B)** Vero E6 cells infected with SARS-CoV-2 at MOI 0.01 were harvested after 24 h and protein extracts were subjected to immunoprecipitation using an anti-DDX3X antibody or an anti-IgG antibody as a negative control (IP CTR). Immunopurified complexes were analyzed by immunoblotting using anti-SARS-CoV Nucleoprotein and anti-DDX3X antibodies. **C)** Vero E6 cells infected with SARS-CoV-2 at MOI 0.01 were fixed after 24 h and analyzed for DDX3X and dsRNA localization by immunofluorescence using specific antibodies. Bottom panel shows colocalization trace profiles. Colocalization rate was measured by Mander's overlap coefficient (MOC) on 25 cells by using ImageJ software. NI: non-infected; N PROTEIN: Nucleoprotein; CoV-2: SARS-CoV-2; CTR: unrelated IgG; dsRNA: double strand RNA. Scale bar, 5 μm. **D)** Vero E6 cells were transfected with small interfering RNAs specific for DDX3X (siDDX3Xa and siDDX3Xb), or non-targeting siRNA (siCTR) as negative control, and infected with SARS-CoV-2 at MOI 0.001. Twenty-four hours later, cells were harvested and DDX3X and viral RNAs were analyzed by RT-qPCR. The graphs report means ± SD of normalized values from three independent experiments. ** = $p < 0.01$, *** = $p < 0.001$. Viral RNA levels are reported as fold changes with respect to the amount detected at 24h post infection.

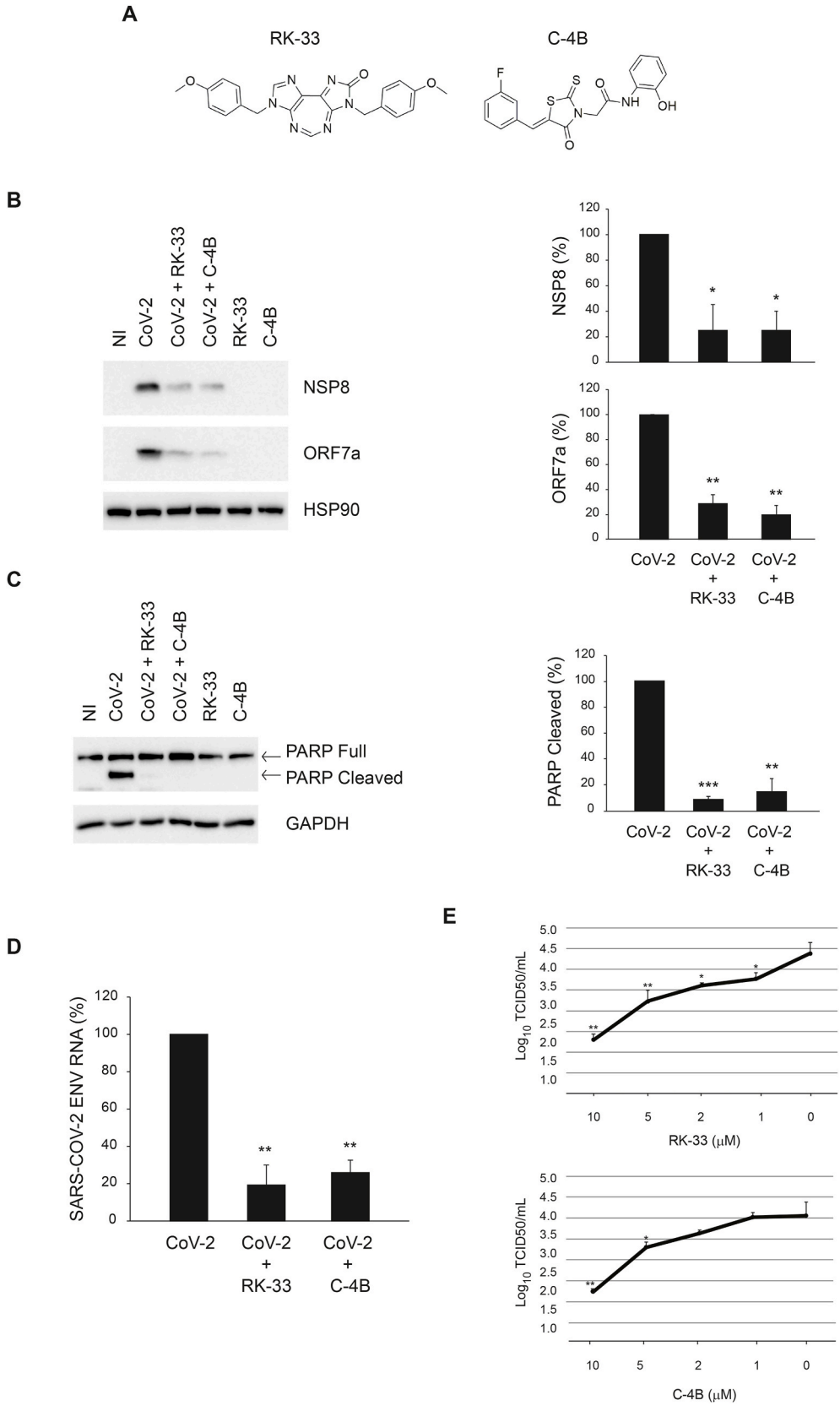

Fig. 4. Inhibition of SARS-CoV-2 infection by RK-33 and C–4B in Vero E6 cells. **A)** Chemical structures of DDX3X inhibitors. **B-D)** Vero E6 cells were infected with SARS-CoV-2 at MOI 0.001 and, at the end of the adsorption period, were treated with RK-33 10 μM, C–4B 10 μM or left untreated, as indicated. At 24 h post infection, cells were harvested and assayed for the levels of SARS-CoV-2 NSP8 and ORF7a proteins (B) and intracellular RNA (D) by immunoblotting and RT-qPCR, respectively. In addition, at 48 h post infection, PARP cleavage was monitored by immunoblotting to evaluate the level of cell death in infected cells (C). HSP90 and GAPDH were included as loading controls. The accompanying graphs report means ± SD of normalized values from three independent experiments. * = $p < 0.05$, ** = $p < 0.01$, *** = $p < 0.001$. Protein and viral RNA levels are reported as fold changes with respect to the amount detected at 24h post infection (p.i.). **E)** Vero E6 cells were infected with SARS-CoV-2 at MOI 0.001. At the end of the adsorption period, cells were treated with RK-33 or C–4B 10 μM, 5 μM, 2 μM, 1 μM or left untreated. Cells and culture media were collected at 24h post infection and subjected to limiting dilution assay on Vero E6 cells. Infectious viral titers are expressed as mean ± SD of Log_{10}TCID50/ml. * = $p < 0.05$, ** = $p < 0.01$. NI: non-infected. CoV-2: SARS-CoV-2.

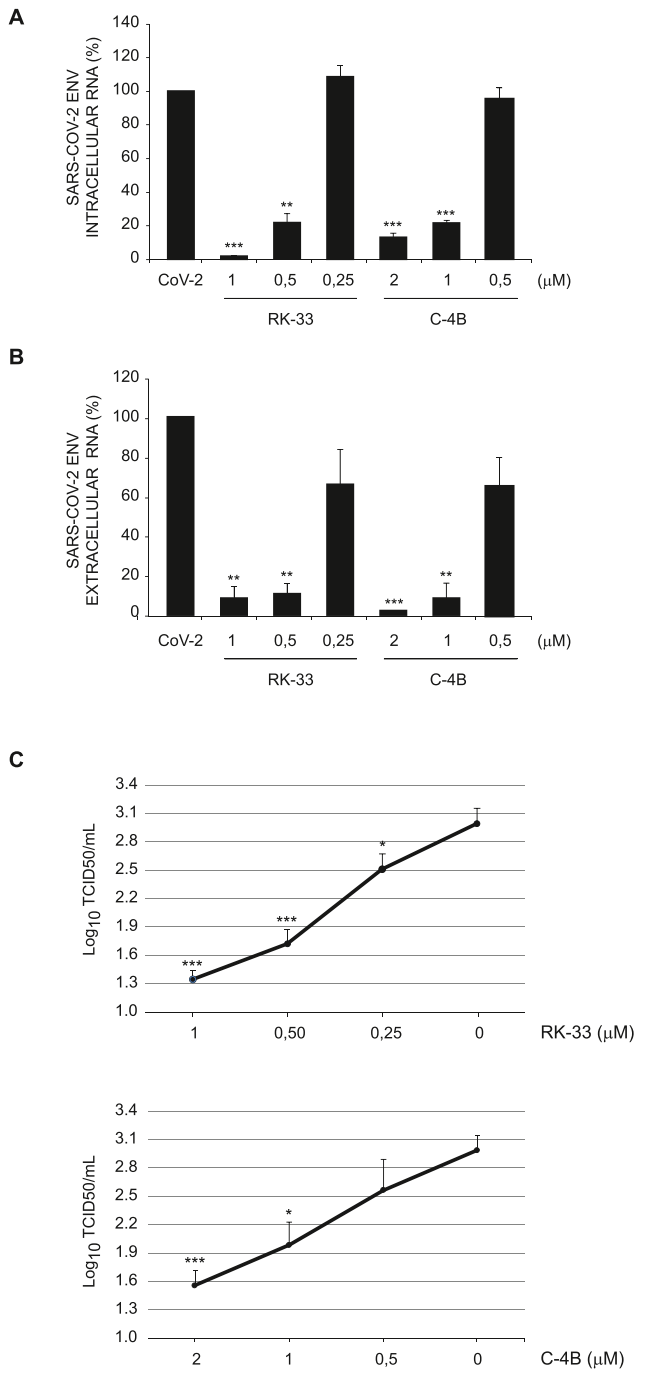

Fig. 5. Inhibition of SARS-CoV-2 infection by RK-33 and C–4B in Calu-3 cells. A-B) Calu-3 cells were infected with SARS-CoV-2 at MOI 0.001 and, at the end of the adsorption period, were treated with RK-33 or C–4B at the indicated concentrations, or left untreated. At 24 h post infection, cells and supernatants were harvested and assayed for intracellular (A) and extracellular (B) RNA, respectively, by RT-qPCR. The graphs report means ± SD of normalized values from three independent experiments. ** = $p < 0.01$, *** = $p < 0.001$. Viral RNA levels are reported as fold changes with respect to the amount detected at 24h post infection. CoV-2: SARS-CoV-2. **C)** Calu-3 cells were infected with SARS-CoV-2 at MOI 0.001. At the end of the adsorption period, cells were treated with RK-33 or C–4B at the indicated concentrations or left untreated. Supernatants were collected at 24h post infection and subjected to limiting dilution assay on Vero E6 cells. Infectious viral titers are expressed as mean ± SD of Log_{10}TCID50/ml. The graphs report means ± SD of normalized values from three independent experiments. * = $p < 0.05$, ** = $p < 0.01$, *** = $p < 0.001$. NI: non-infected.

B). The antiviral effect of DDX3X inhibitors was also confirmed when the infectivity of viral particles produced in cells treated with different concentrations of RK-33 or C–4B was measured by limiting dilution assay (Fig. 5C).

4. Discussion

Virus-host interaction represents an ongoing evolutionary arms race accomplished at molecular and cellular levels, whose in-depth characterization can unveil sensitive targets to stop infections (de Chassey et al., 2014). Here, we used a mass spectrometry-based approach to study the interactome of SARS-CoV-2 Nucleoprotein in infected cells. We identified the interaction of Nucleoprotein with ribosomal proteins and a number of proteins involved in RNA metabolism, including factors regulating stress granule assembly. The interaction of Nucleoprotein with stress granule components was recently identified in a interactome study performed by Gordon and colleagues upon overexpression of single SARS-CoV-2 proteins (Gordon et al., 2020). Here, using an infectious cell system, we confirmed that some of these interactions, e.g. G3BP1, occur in infected cells, and identified additional factors, e.g. DDX3X, playing a role in SARS-CoV-2 infection.

Stress granules are cytoplasmic aggregates of the translation preinitiation complex 48S, which accumulate in response to inhibition of translation initiation induced by stress signals often resulting in eIF2α phosphorylation (Protter and Parker, 2016). Stress granule formation is an integral part of antiviral response aimed at blocking viral gene expression (Tsai and Lloyd, 2014). In addition, stress granules can function as novel signaling platforms and regulate antiviral response pathways (McCormick and Khaperskyy, 2017).

Interestingly, we found that Nucleoprotein interacts with the scaffold proteins of stress granules, such as G3BP1, G3BP2, IGF2BP2, IGF2BP3 and YBX1, but other components typical of this type of aggregate, such as eukaryotic initiation factors, were not detected, suggesting that Nucleoprotein does not associate with the entire assembled structure. Indeed, the analysis of the distribution of G3BP1 in infected cells showed that this protein is not present in dotted structures. Importantly, downregulation of G3BP1 expression results in a decrease of viral replication, suggesting that SARS-CoV-2 hijacks stress granule components for its life cycle. Absence of stress granules in infected cells was also confirmed when the distribution of eIF4G and the levels of eIF2α phosphorylation were analyzed. Whether Nucleoprotein interferes with stress granule formation through the direct interaction with scaffold proteins or by binding and modulating the activity of the eIF2α phosphatase PP1 remains to be determined. Conversely, we observed that stress granules and high levels of eIF2α phosphorylation are present in neighbouring non-infected cells. This result suggests that infected cells release signals able to induce stress granules in non-cell-autonomous manner, as described in other pathological conditions (Hu et al., 2010; Grabocka and Bar-Sagi, 2016).

Among Nucleoprotein interacting proteins involved in stress granule dynamics, we identified DDX3X as a "druggable" target required for SARS-CoV-2 replication. DDX3X belongs to the large DEAD-box family of ATP-dependent RNA helicases and plays a role in several aspects of RNA metabolism, such as transcription, splicing, mRNA export and initiation of translation (Ariumi, 2014). Multiple lines of evidence point at a role of DDX3X in viral infection (Valiente-Echeverría et al., 2015) as either a cofactor of viral replication or a mediator of the innate immunity system. DDX3X regulates the replication of viruses belonging to different families, such as HCV, Dengue, West Nile, HIV-1, HBV, Vaccinia, Norovirus and influenza A virus, by interacting with both viral RNA and viral proteins (Valiente-Echeverría et al., 2015). In particular, it is well characterized its role in HIV infection where, by unfolding viral RNA secondary structures, DDX3X enhances both nucleus-to-cytoplasm transport and translation of HIV genome (Stunnenberg et al., 2018). In apparent contradiction with its proviral functions, DDX3X participates in antiviral signaling pathways by regulating the activity of TBK1, IKKε and MAVS (Soulat et al., 2008; Fullam

and Schröder, 2013; Oshiumi et al., 2010).

Here, we provided evidence that DDX3X interacts with Nucleoprotein, localizes with cytoplasmic viral RNA foci and is required for SARS-CoV-2 infection in Vero E6 and Calu-3 cells. Indeed, treatment of cells with two independent DDX3X inhibitors, RK-33 and C–4B, results in a significant inhibition of SARS-CoV-2 replication and viral production. Although we cannot rule out that DDX3X inhibitors may also target other DEAD RNA helicases, as reported for DDX1 at high micromolar concentration (Maga et al., 2011), the results obtained both in the dose-response experiments and using small interfering RNAs corroborate a direct involvement of DDX3X in SARS-CoV-2 infection.

Based on these results, we hypothesize that, by preventing stress granule formation, Nucleoprotein can make DDX3X available to unfold SARS-CoV-2 RNA secondary structures and facilitate viral translation and replication. Notably, evidence of DDX3X association with SARS-CoV-2 RNA has been recently reported in a RNA interactome study (Schmidt et al., 2021). In addition, Nucleoprotein could interact with DDX3X to inhibit its activity in antiviral response Winnard Jr. et al., 2021.

5. Conclusions

Altogether, these results identify DDX3X as an attractive target for host-directed therapy to limit SARS-CoV-2 infection. Recently, novel DDX3X inhibitors aimed at inhibiting HIV infection have been developed showing optimal tolerability and biodistribution, which represent good candidates for clinical studies (Brai et al., 2020). Moreover, the presence of DHX9 and DDX21 (Gordon et al., 2020) in the Nucleoprotein interactome suggests that multiple RNA helicases are potential candidates as host targets to halt SARS-CoV-2 replication.

Acknowledgements

This work was supported in part by grants from Ricerca Corrente and COVID-2020-12371817 by the Ministry of Health, donation from “Avvocati e Procuratori dello Stato”, AIRC (IG2015 n. 17404 to GMF, IG2018-21880 to M.P.), “Beyond Borders” University of Rome “Tor Vergata” and Regione Lazio (Gruppi di ricerca, E56C18000460002, to M.P.) and from the European Commission – Horizon 2020 (European Virus Archive GLOBAL –– 871029 and EU project 101003551 - EXSCALATE4CoV). The authors also acknowledge the support of the grant from the Russian Government Program for the Recruitment of the Leading Scientists into the Russian Institutions of Higher Education (14. W03.31.0029 to M.P.)

Appendix A. Supplementary data

Supplementary data to this article can be found online at https://doi.org/10.1016/j.antiviral.2021.105064.

Author contributions

Conceptualization, G.M.F.; Investigation: F.Ci., M.D.R., A.R., F.Co., G.R.; Compound synthesis: A.B., F.M., L.B.; data analysis: C. A., F. M., C. C., M. R. C., L. B., G. I. M.P. G.M.F.; Writing – Original Draft, F.Ci., M.D. R., and G.M.F.; Writing –Review & Editing, A.R., C. A., F. M., C. C., M. R. C., L. B., G. I. M.P. Funding Acquisition, M. R. C., G. I., M.P., G.M.F.

Declaration of interests

The authors declare that they have no conflict of interest.

References

Ariumi, Y., 2014. Multiple functions of DDX3 RNA helicase in gene regulation, tumorigenesis, and viral infection. Front. Genet. 5, 423. https://doi.org/10.3389/fgene.2014.00423.

Brai, A., Riva, V., Saladini, F., Zamperini, C., Trivisani, C.I., Garbelli, A., Pennisi, C., Giannini, A., Boccuto, A., Bugli, F., Martini, M., Sanguinetti, M., Zazzi, M., Dreassi, E., Botta, M., Maga, G., 2020. DDX3X inhibitors, an effective way to overcome HIV-1 resistance targeting host proteins. S0223-5234(20)30288-9 Eur. J. Med. Chem. 200, 112319 [pii].

Brai, A., Martelli, F., Riva, V., Garbelli, A., Fazi, R., Zamperini, C., Pollutri, A., Falsitta, L., Ronzini, S., Maccari, L., Maga, G., Giannecchini, S., Botta, M., 2019. DDX3X helicase inhibitors as a new strategy to fight the West Nile virus infection. J. Med. Chem. 62, 2333–2347. https://doi.org/10.1021/acs.jmedchem.8b01403.

Cui, J., Li, F., Shi, Z.L., 2019. Origin and evolution of pathogenic coronaviruses. Nat. Rev. Microbiol. 17, 181–192. https://doi.org/10.1038/s41579-018-0118-9.

de Chassey, B., Meyniel-Schicklin, L., Vonderscher, J., André, P., Lotteau, V., 2014. Virus-host interactomics: new insights and opportunities for antiviral drug discovery, 115-014-0115-1 Genome Med. 6. https://doi.org/10.1186/s13073-014-0115-1. eCollection 2014.

de Wilde, A.H., Snijder, E.J., Kikkert, M., van Hemert, M.J., 2018. Host factors in coronavirus replication. Curr. Top. Microbiol. Immunol. 419, 1–42. https://doi.org/10.1007/82_2017_25.

Di Rienzo, M., Antonioli, M., Fusco, C., Liu, Y., Mari, M., Orhon, I., Refolo, G., Germani, F., Corazzari, M., Romagnoli, A., Ciccosanti, F., Mandriani, B., Pellico, M. T., De La Torre, R., Ding, H., Dentice, M., Neri, M., Ferlini, A., Reggiori, F., Kulesz-Martin, M., Piacentini, M., Merla, G., Fimia, G.M., 2019. Autophagy induction in atrophic muscle cells requires ULK1 activation by TRIM32 through unanchored K63-linked polyubiquitin chains. Sci. Adv. 5, eaau8857 https://doi.org/10.1126/sciadv.aau8857.

Fullam, A., Schröder, M., 2013. DExD/H-box RNA helicases as mediators of anti-viral innate immunity and essential host factors for viral replication. Biochim. Biophys. Acta 1829, 854–865. S1874-9399(13)00057-6.

Fung, T.S., Liu, D.X., 2019. Human coronavirus: host-pathogen interaction. Annu. Rev. Microbiol. 73, 529–557. https://doi.org/10.1146/annurev-micro-020518-115759.

Gordon, D.E., Jang, G.M., Bouhaddou, M., Xu, J., Obernier, K., O'Meara, M.J., Guo, J.Z., Swaney, D.L., Tummino, T.A., Huttenhain, R., Kaake, R.M., Richards, A.L., Tutuncuoglu, B., Foussard, H., Batra, J., Haas, K., Modak, M., Kim, M., Haas, P., Polacco, B.J., Braberg, H., Fabius, J.M., Eckhardt, M., Soucheray, M., Bennett, M.J., Cakir, M., McGregor, M.J., Li, Q., Naing, Z.Z.C., Zhou, Y., Peng, S., Kirby, I.T., Melnyk, J.E., Chorba, J.S., Lou, K., Dai, S.A., Shen, W., Shi, Y., Zhang, Z., Barrio-Hernandez, I., Memon, D., Hernandez-Armenta, C., Mathy, C.J.P., Perica, T., Pilla, K. B., Ganesan, S.J., Saltzberg, D.J., Ramachandran, R., Liu, X., Rosenthal, S.B., Calviello, L., Venkataramanan, S., Lin, Y., Wankowicz, S.A., Bohn, M., Trenker, R., Young, J.M., Cavero, D., Hiatt, J., Roth, T., Rathore, U., Subramanian, A., Noack, J., Hubert, M., Roesch, F., Vallet, T., Meyer, B., White, K.M., Miorin, L., Agard, D., Emerman, M., Ruggero, D., Garcia-Sastre, A., Jura, N., von Zastrow, M., Taunton, J., Schwartz, O., Vignuzzi, M., d'Enfert, C., Mukherjee, S., Jacobson, M., Malik, H.S., Fujimori, D.G., Ideker, T., Craik, C.S., Floor, S., Fraser, J.S., Gross, J., Sali, A., Kortemme, T., Beltrao, P., Shokat, K., Shoichet, B.K., Krogan, N.J., 2020. A SARS-CoV-2-human protein-protein interaction map reveals drug targets and potential, 2020.03.22.002386 Drug-Repurposing. bioRxiv.

Grabocka, E., Bar-Sagi, D., 2016. Mutant KRAS enhances tumor cell fitness by upregulating stress granules. S0092-8674(16)31607-5 Cell 167, 1803–1813. e12.

Hartenian, E., Nandakumar, D., Lari, A., Ly, M., Tucker, J.M., Glaunsinger, B.A., 2020. The molecular virology of Coronaviruses. J. Biol. Chem. jbc.REV120.013930.

Hoffmann, M., Mosbauer, K., Hofmann-Winkler, H., Kaul, A., Kleine-Weber, H., Kruger, N., Gassen, N.C., Muller, M.A., Drosten, C., Pohlmann, S., 2020. Chloroquine does not inhibit infection of human lung cells with SARS-CoV-2. Nature. https://doi.org/10.1038/s41586-020-2575-3.

Hu, S., Claud, E.C., Musch, M.W., Chang, E.B., 2010. Stress granule formation mediates the inhibition of colonic Hsp70 translation by interferon-gamma and tumor necrosis factor-alpha. Am. J. Physiol. Gastrointest. Liver Physiol. 298, G481–G492. https://doi.org/10.1152/ajpgi.00234.2009.

Kim, D., Lee, J.Y., Yang, J.S., Kim, J.W., Kim, V.N., Chang, H., 2020. The architecture of SARS-CoV-2 transcriptome. S0092-8674(20)30406-2 Cell 181, 914–921. e10.

Kukhanova, M.K., Karpenko, I.L., Ivanov, A.V., 2020. DEAD-box RNA helicase DDX3: functional properties and development of DDX3 inhibitors as antiviral and anticancer drugs, 10.3390/molecules25041015 Molecules 25, 1015, 10.3390/molecules25041015.

Lei, X., Dong, X., Ma, R., Wang, W., Xiao, X., Tian, Z., Wang, C., Wang, Y., Li, L., Ren, L., Guo, F., Zhao, Z., Zhou, Z., Xiang, Z., Wang, J., 2020. Activation and evasion of type I interferon responses by SARS-CoV-2. Nat. Commun. 11 https://doi.org/10.1038/s41467-020-17665-9, 3810-020-17665-9.

Liu, D.X., Fung, T.S., Chong, K.K., Shukla, A., Hilgenfeld, R., 2014. Accessory proteins of SARS-CoV and other coronaviruses. Antivir. Res. 109, 97–109. https://doi.org/10.1016/j.antiviral.2014.06.013.

Luo, H., Chen, Q., Chen, J., Chen, K., Shen, X., Jiang, H., 2005. The nucleocapsid protein of SARS coronavirus has a high binding affinity to the human cellular heterogeneous nuclear ribonucleoprotein A1. S0014-5793(05)00432-1 FEBS Lett. 579, 2623–2628.

Maga, G., Falchi, F., Radi, M., Botta, L., Casaluce, G., Bernardini, M., Irannejad, H., Manetti, F., Garbelli, A., Samuele, A., Zanoli, S., Esté, J.A., Gonzalez, E., Zucca, E., Paolucci, S., Baldanti, F., De Rijck, J., Debyser, Z., Botta, M., 2011. Toward the discovery of novel anti-HIV drugs. Second-generation inhibitors of the cellular ATPase DDX3 with improved anti-HIV activity: synthesis, structure-activity relationship analysis, cytotoxicity studies, and target validation. ChemMedChem 6, 1371–1389. https://doi.org/10.1002/cmdc.201100166.

McCormick, C., Khaperskyy, D.A., 2017. Translation inhibition and stress granules in the antiviral immune response. Nat. Rev. Immunol. 17, 647–660. https://doi.org/10.1038/nri.2017.63.

Ortiz-Prado, E., Simbana-Rivera, K., Gomez-Barreno, L., Rubio-Neira, M., Guaman, L.P., Kyriakidis, N.C., Muslin, C., Jaramillo, A.M.G., Barba-Ostria, C., Cevallos-Robalino, D., Sanches-SanMiguel, H., Unigarro, L., Zalakeviciute, R., Gadian, N., Lopez-Cortes, A., 2020. Clinical, molecular, and epidemiological characterization of the SARS-CoV-2 virus and the Coronavirus Disease 2019 (COVID-19), a comprehensive literature review. S0732-8893(20)30471-5 Diagn. Microbiol. Infect. Dis. 98, 115094.

Oshiumi, H., Sakai, K., Matsumoto, M., Seya, T., 2010. DEAD/H BOX 3 (DDX3) helicase binds the RIG-I adaptor IPS-1 to up-regulate IFN-beta-inducing potential. Eur. J. Immunol. 40, 940–948. https://doi.org/10.1002/eji.200940203.

Pislar, A., Mitrovic, A., Sabotic, J., Pecar Fonovic, U., Perisic Nanut, M., Jakos, T., Senjor, E., Kos, J., 2020. The role of cysteine peptidases in coronavirus cell entry and replication: the therapeutic potential of cathepsin inhibitors. PLoS Pathog. 16, e1009013 https://doi.org/10.1371/journal.ppat.1009013.

Protter, D.S.W., Parker, R., 2016. Principles and properties of stress granules. Trends Cell Biol. 26, 668–679. S0962-8924(16)30047-2.

Refolo, G., Ciccosanti, F., Di Rienzo, M., Basulto Perdomo, A., Romani, M., Alonzi, T., Tripodi, M., Ippolito, G., Piacentini, M., Fimia, G.M., 2019. Negative regulation of mitochondrial antiviral signaling protein-mediated antiviral signaling by the mitochondrial protein LRPPRC during hepatitis C virus infection. Hepatology 69, 34–50. https://doi.org/10.1002/hep.30149.

Romagnoli, A., Petruccioli, E., Palucci, I., Camassa, S., Carata, E., Petrone, L., Mariano, S., Sali, M., Dini, L., Girardi, E., Delogu, G., Goletti, D., Fimia, G.M., 2018. Clinical isolates of the modern Mycobacterium tuberculosis lineage 4 evade host defense in human macrophages through eluding IL-1beta-induced autophagy. Cell Death Dis. 9 https://doi.org/10.1038/s41419-018-0640-8, 624-018-0640-8.

Sa Ribero, M., Jouvenet, N., Dreux, M., Nisole, S., 2020. Interplay between SARS-CoV-2 and the type I interferon response. PLoS Pathog. 16, e1008737 https://doi.org/10.1371/journal.ppat.1008737.

Sauvat, A., Ciccosanti, F., Colavita, F., Di Rienzo, M., Castilletti, C., Capobianchi, M.R., Kepp, O., Zitvogel, L., Fimia, G.M., Piacentini, M., Kroemer, G., 2020. On-target versus off-target effects of drugs inhibiting the replication of SARS-CoV-2, 656-020-02842-x Cell Death Dis. 11, 10.1038/s41419-020-02842-x.

Schmidt, N., Lareau, C.A., Keshishian, H., Ganskih, S., Schneider, C., Hennig, T., Melanson, R., Werner, S., Wei, Y., Zimmer, M., Ade, J., Kirschner, L., Zielinski, S., Dolken, L., Lander, E.S., Caliskan, N., Fischer, U., Vogel, J., Carr, S.A., Bodem, J., Munschauer, M., 2021. The SARS-CoV-2 RNA-protein interactome in infected human cells. Nat. Microbiol. 6, 339–353. https://doi.org/10.1038/s41564-020-00846-z.

Siu, Y.L., Teoh, K.T., Lo, J., Chan, C.M., Kien, F., Escriou, N., Tsao, S.W., Nicholls, J.M., Altmeyer, R., Peiris, J.S., Bruzzone, R., Nal, B., 2008. The M, E, and N structural proteins of the severe acute respiratory syndrome coronavirus are required for efficient assembly, trafficking, and release of virus-like particles. J. Virol. 82, 11318–11330. https://doi.org/10.1128/JVI.01052-08.

Snijder, E.J., Limpens, R.W.A.L., de Wilde, A.H., de Jong, A.W.M., Zevenhoven-Dobbe, J.C., Maier, H.J., Faas, F.F.G.A., Koster, A.J., Barcena, M., 2020. A unifying structural and functional model of the coronavirus replication organelle: tracking down RNA synthesis. PLoS Biol. 18, e3000715 https://doi.org/10.1371/journal.pbio.3000715.

Soulat, D., Bürckstümmer, T., Westermayer, S., Goncalves, A., Bauch, A., Stefanovic, A., Hantschel, O., Bennett, K.L., Decker, T., Superti-Furga, G., 2008. The DEAD-box helicase DDX3X is a critical component of the TANK-binding kinase 1-dependent innate immune response. EMBO J. 27, 2135–2146. https://doi.org/10.1038/emboj.2008.126.

Stertz, S., Reichelt, M., Spiegel, M., Kuri, T., Martinez-Sobrido, L., Garcia-Sastre, A., Weber, F., Kochs, G., 2007. The intracellular sites of early replication and budding of SARS-coronavirus. S0042-6822(06)00876-2 Virology 361, 304–315.

Stunnenberg, M., Geijtenbeek, T.B.H., Gringhuis, S.I., 2018. DDX3 in HIV-1 infection and sensing: a paradox. Cytokine Growth Factor Rev. 40, 32–39. S1359-6101(18)30033-9.

Szklarczyk, D., Gable, A.L., Lyon, D., Junge, A., Wyder, S., Huerta-Cepas, J., Simonovic, M., Doncheva, N.T., Morris, J.H., Bork, P., Jensen, L.J., Mering, C.V., 2019. STRING v11: protein-protein association networks with increased coverage, supporting functional discovery in genome-wide experimental datasets. Nucleic Acids Res. 47, D607–D613. https://doi.org/10.1093/nar/gky1131.

Tsai, W.C., Lloyd, R.E., 2014. Cytoplasmic RNA granules and viral infection. Annu. Rev. Virol. 1, 147–170. https://doi.org/10.1146/annurev-virology-031413-085505.

Tyanova, S., Temu, T., Sinitcyn, P., Carlson, A., Hein, M.Y., Geiger, T., Mann, M., Cox, J., 2016. The Perseus computational platform for comprehensive analysis of (prote) omics data. Nat. Methods 13, 731–740. https://doi.org/10.1038/nmeth.3901.

Valiente-Echeverría, F., Hermoso, M.A., Soto-Rifo, R., 2015. RNA helicase DDX3: at the crossroad of viral replication and antiviral immunity. Rev. Med. Virol. 25, 286–299. https://doi.org/10.1002/rmv.1845.

Weber, F., Wagner, V., Rasmussen, S.B., Hartmann, R., Paludan, S.R., 2006. Double-stranded RNA is produced by positive-strand RNA viruses and DNA viruses but not in detectable amounts by negative-strand RNA viruses. J. Virol. 80, 5059–5064, 80/10/5059.

Winnard Jr, P.T., Vesuna, F., Raman, V., 2021. Targeting host DEAD-box RNA helicase DDX3X for treating viral infections. Antivir. Res. 185, 104994. https://doi.org/10.1016/j.antiviral.2020.104994.

Wu, C.H., Chen, P.J., Yeh, S.H., 2014. Nucleocapsid phosphorylation and RNA helicase DDX1 recruitment enables coronavirus transition from discontinuous to continuous transcription. Cell Host Microbe 16, 462–472. https://doi.org/10.1016/j.chom.2014.09.009.

Yang, S.N.Y., Atkinson, S.C., Audsley, M.D., Heaton, S.M., Jans, D.A., Borg, N.A., 2020. RK-33 is a broad-spectrum antiviral agent that targets DEAD-box RNA helicase DDX3X. Cells 9, 170. https://doi.org/10.3390/cells9010170.